NPS-61-90-001

NAVAL POSTGRADUATE SCHOOL

Monterey, California

FREQUENCY CONTENT OF COHERENT CHERENKOV RADIATION

JOHN R. NEIGHBOURS
FRED R. BUSKIRK
XAVIER K. MARUYAMA

NOVEMBER 1989

Technical Report

Prepared for:
Naval Postgraduate School, Monterey, CA 93943-5000 and
Space and Naval Warfare Systems Command, Washington, D.C.
20363-5100 and Defense Advanced Research Projects Agency
Arlington, VA 22209-2308

NAVAL POSTGRADUATE SCHOOL
Monterey, California

Rear Admiral R. W. West, Jr.
Superintendent

Harrison Shull
Provost

The work summarized herein was supported by the Naval Postgraduate School and partially by funds provided by the Defense Advanced Research Projects Agency, Arlington, Virginia. Reproduction of all or part of this report is authorized.

This report was edited by:

REPORT DOCUMENTATION PAGE

REPORT SECURITY CLASSIFICATION UNCLASSIFIED	1b RESTRICTIVE MARKINGS
SECURITY CLASSIFICATION AUTHORITY	3 DISTRIBUTION / AVAILABILITY OF REPORT Approved for public release; distribution is unlimited.
DECLASSIFICATION / DOWNGRADING SCHEDULE	
PERFORMING ORGANIZATION REPORT NUMBER(S) NPS-61-90-001	5 MONITORING ORGANIZATION REPORT NUMBER(S)
NAME OF PERFORMING ORGANIZATION Naval Postgraduate School 6b OFFICE SYMBOL (*If applicable*) 61	7a NAME OF MONITORING ORGANIZATION
ADDRESS (*City, State, and ZIP Code*) Monterey, CA 93943-5000	7b ADDRESS (*City, State, and ZIP Code*)
NAME OF FUNDING / SPONSORING ORGANIZATION Defense Advanced Research Projects Agency 8b OFFICE SYMBOL (*If applicable*)	9 PROCUREMENT INSTRUMENT IDENTIFICATION NUMBER N6227118RWR80063 O&MN, Direct Funding
ADDRESS (*City, State, and ZIP Code*) 1400 Wilson Blvd Arlington, VA 22209-2308	10 SOURCE OF FUNDING NUMBERS PROGRAM ELEMENT NO / PROJECT NO / TASK NO / WORK UNIT ACCESSION NO.

TITLE (*Include Security Classification*)
Frequency Content of Coherent Cherenkov Radiation

PERSONAL AUTHOR(S)
John R. Neighbours, Fred R. Buskirk, Xavier K. Maruyama

13a TYPE OF REPORT	13b TIME COVERED	14 DATE OF REPORT (*Year, Month, Day*)	15 PAGE COUNT
Technical Report	FROM NOV88 TO NOV89	891108	37

SUPPLEMENTARY NOTATION

COSATI CODES		
FIELD	GROUP	SUB-GROUP

18 SUBJECT TERMS (*Continue on reverse if necessary and identify by block number*)
Radiation from Electron Beam
Cherenkov Radiation

ABSTRACT (*Continue on reverse if necessary and identify by block number*)
At constant beam energy and propagation angle, the coherent radiation from a charged particle beam is a function of frequency only. The intensity of the radiation oscillates with a frequency dependent on the length of the path of the beam and is modulated by the form factor corresponding to the shape of an individual charge bunch. Calculations are presented for line charge distributions which have rectangular, triangular, and trapezoidal axial variation. A point charge distribution is also considered for comparison.

DISTRIBUTION / AVAILABILITY OF ABSTRACT ☒ UNCLASSIFIED/UNLIMITED ☐ SAME AS RPT ☐ DTIC USERS	21 ABSTRACT SECURITY CLASSIFICATION UNCLASSIFIED
22a NAME OF RESPONSIBLE INDIVIDUAL Professor J.R. Neighbours	22b TELEPHONE (*Include Area Code*) (408)646-2922 22c OFFICE SYMBOL 61Nb

☆ U.S. Government Printing Office: 1986—606-24.

FREQUENCY CONTENT OF COHERENT CHERENKOV RADIATION

John R. Neighbours

Fred R. Buskirk

Xavier K. Maruyama

Naval Postgraduate School

Monterey, California 93943

ABSTRACT

At constant beam energy and propagation angle, the coherent radiation from a charged particle beam is a function of frequency only. The intensity of the radiation oscillates with a frequency dependant on the length of the path of the beam and is modulated by the form factor corresponding to the shape of an individual charge bunch. Calculations are presented for line charge distributions which have rectangular, triangular, and trapezoidal axial variation. A point charge distribution is also considered for comparison.

INTRODUCTION

In previous work, we have discussed the spatial distribution of Cherenkov and sub–Cherenkov radiation from a charged particle beam in detail[1-4], giving both a diffraction and an envelope[5] form. The radiation is polarized with the electric vector lying in the plane of the observer and the direction of propagation of the beam. Both the power radiated from a beam of periodic charge bunches and the energy radiated by a single bunch have the same functional form.

The distance of propagation of the beam is shown to be a critical parameter which affects the onset of Cherenkov radiation as well as the shifting and broadening of the Cherenkov cone. At short path lengths, the radiation occurs at substanially lower energies and the radiation pattern is quite broad. As the path length increases, the phase matching condition between the charge bunch and the wave becomes more stringent so that the energy threshold rises. Concomitantly, the main cone angle approaches the Cherenkov angle with an increasing fraction of the total radiation being radiated at that angle.

Our experimental studies[1 3 6] of coherent microwave Cherenkov radiation were carried out with traditional relatively narrow banded X and K band horns, wavegiudes, and narrow band filters. Along with these experiments, the analysis was performed with the implicit idea of using narrow band detectors with which the radiation patterns could be scanned. Now, with the advent of broadband antennas[7], experimental studies of the frequency distribution of the radiation become possible. This paper presents predictions which should be compared to the results of future experiments.

FREQUENCY DEPENDENCE

The radiation from a charged particle beam has been calculated previously under the assumption that the bunches in the beam are unchanging in shape and size as the beam travels through the medium with a velocity $v = \beta c_0$, where c_0 is the speed of light in vacuum. The results are that the coherent radiated power per unit solid angle from a periodic charged particle beam traveling a finite distance L at constant velocity is

$$W(\nu,\mathbf{k}) = \nu_0^2 Q R^2 \tag{1}$$

where ν_0 is the fundamental frequency of the beam generator and ν is a harmonic of of ν_0. Similarly, E $d\nu$, the energy radiated per unit solid angle within the frequency range $d\nu$ by a single bunch of charge traveling a distance L is

$$\mathcal{E}(\nu,\mathbf{k})\, d\nu = Q R^2\, d\nu \tag{2}$$

The constant Q, and the radiation function R are the same in both cases.

$$Q = \mu c q^2 / 8\pi^2 \tag{3}$$

Here μ is the permeability of the medium, q is the charge of an individual bunch, and the velocity of light in the medium is $c = c_0/n$, where n is the index of refraction. The radiation function R, which includes diffraction effects associated with the path length is defined to be

$$R = 2\,\pi\,\eta \sin\theta\, I(u)\, F(\mathbf{k}), \tag{4}$$

where θ is the angle between the direction of travel of the charged particle beam and the direction of propagation of the emitted radiation, the form factor $F(\mathbf{k})$ is given by the Fourier transform of the charge distribution of an individual bunch, and $I(u) = \text{sinc } u$ is the diffraction function. The diffraction variable u is given by

$$u = \pi\,\eta\,[(1/n\beta) - \cos\theta\,] \tag{5}$$

where $\eta = L/\lambda$ is the ratio of the path length of the charged particle beam to the wavelength in the medium of the emitted radiation.

In our previous work, the emphasis has been on the angular distribution of radiation at a given frequency, for which the diffraction form is well suited. In this paper the discussion concentrates on the frequency dependence of the radiation at a fixed angle with the objective of clarifying how the beam parameters such as path length, bunch length, and rise time may be determined from measurements of the radiation. For the present discussion, it is more convenient to use the envelope form of the radiation function

$$R = 2\, G(n\beta,\theta)\, F(\mathbf{k}) \sin u \tag{6}$$

in which the spatial envelope function, $G(n\beta,\theta)$ is defined as

$$G(n\beta,\theta) = \sin\theta\, [(n\beta)^{-1} - \cos\theta]^{-1} \tag{7}$$

We have already noted[5] that both the radiated power W, and the radiated energy E, can be visualized as an oscillatory spatial function modulated by the envelope G^2. In the sub–Cherenkov regime ($n\beta < 1$), the envelope has a maximum of $\cot^2\theta_s$ where $\cos\theta_s = n\beta$. In the Cherenkov regime ($n\beta > 1$) the envelope has a singularity at the Cherenkov angle θ_c ($\cos\theta_c = 1/n\beta$), but since this occurs at the Cherenkov angle where u=0, $R^2(\theta_c)$ has a finite maximum . In both regimes, G^2 has zeroes at $\theta = 0$ and $\theta = \pi$. Figure 1 from reference 5 shows G^2 for both regimes.

Assuming no dispersion i.e. $c = \nu\lambda$, the diffraction variable can be written in terms of frequency as

$$u = \pi\, [(1/n\beta) - \cos\theta\,]\, (\nu/f_0) \tag{8}$$

where, for convenience, the path length frequency, f_0, is defined in terms of the distance through which the charged particle beam propagates.

$$f_0 = c/L \tag{9}$$

The charge distribution of a single bunch is $\rho(\mathbf{r})$ and $F(\mathbf{k})$ is the dimensionless form factor defined by

$$\rho(\mathbf{k}) = q\, F(\mathbf{k}) \tag{10}$$

where the Fourier components of the charge are

$$\rho(\mathbf{k}) = \iiint_{-\infty}^{\infty} \rho(\mathbf{r})\, e^{i\,\mathbf{k}\,\mathbf{r}}\, d^3 r \tag{11}$$

The particular expression for the form factor depends upon the details of the charge distribution. However, since the wave vector of the emitted radiation is $\mathbf{k}$, and in the dispersionless approximation, $k = 2\pi\nu/c$, the form factor can be written as a function of frequency. Although it is not necessary in the formalism, we have usually dealt with charges having cylindrical symmetry about the beam propagation direction which results in radiation patterns that also have cylindrical symmetry. This seems to be a good first approximation for a stable beam and simplifies the analysis.

The radiation function can be expressed as a function of frequency by substituting (8) into (6) and writing $F(\mathbf{k})$ explicitly as a function of frequency. Since both the radiated power and the radiated energy are proportional to R^2, it is more convenient to deal with the square of the radiation function.

$$R^2(n\beta,\theta,\nu) = 4\, G^2(n\beta,\theta)\, \sin^2(a\nu)\, F^2(\nu) \tag{12}$$

where

$$a = [(n\beta)^{-1} - \cos\,\theta\,]\,(\pi/f_0) \tag{13}$$

At constant beam energy and constant propagation direction of the emitted radiation, the term in square brackets in (13) is constant so that a is a parameter whose value depends on the path length of the beam through f_0. Also, under these conditions, the envelope function, G^2 is constant and consequently the square of the radiation function, (12), is a function of frequency only. Aside from a constant, $R^2(n\beta,\theta,\nu)$ is the frequency distribution of radiation emitted at the angle θ from a charged particle beam of relative velocity $\beta' = n\beta$.

Thus, the radiation at constant beam energy and propagation angle consists of an oscillating $\sin^2(a\nu)$ function whose envelope, $F^2(\nu)$, is the square of the form factor.

The "frequency" of the oscillations in the Cherenkov radiation is a/π which has the dimensions of Hz^{-1}. However this terminology leads to some confusion. Instead of "frequency" and "period", we use the terms null density for a/π and null separation for its reciprocal.

The $\sin^2(a\nu)$ function has equally spaced zeroes whose null separation $\Delta\nu_P = \pi/a$ is the spacing of the oscillations in the frequency distribution which result from the finite path length of the charged particle beam. Normalized to f_0, the null separation is

$$\frac{\Delta\nu_P}{f_0} = [(n\beta)^{-1} - \cos\theta]^{-1} \tag{14}$$

which has a singularity at the Cherenkov angle. However, the normalized null density

$$\frac{f_0}{\Delta\nu_P} = [(n\beta)^{-1} - \cos\theta] \tag{14A}$$

is finite throughout the entire angular range for both the Cherenkov and sub–Cherenkov regimes. Fig (2) is a graph of the null density as a function of angle for values of $n\beta$ above and below the Cherenkov limit.

The oscillations of the frequency distribution of the radiation are of increasing "frequency" as the angle of propagation moves toward the back direction, *i.e.*, the null density increases as the angle of propagation increases. In both regimes, the null density has the relatively small value of $((1/n\beta)-1)$ in the forward direction, continues to be small for small angles, and then increases to a value of $((1/n\beta)+1)$ at $\theta=\pi$. In the Cherenkov regime, the null density passes through zero at the Cherenkov angle, there is no oscillation in the frequency distribution when the radiation propagates at this angle. This effect is a consequence of the well known result that at the Cherenkov angle, the radiation remains in phase with the charge for all frequencies so that the radiation has no frequency dependence.

In the sub–Cherenkov regime, a is never zero so that the frequency distribution of radiation is always oscillatory. In the Cherenkov regime, a goes to zero at the Cherenkov angle, and the spatial envelope, G^2 has a singularity. However, as noted earlier, in this

case the square of the radiation function is finite and depends explicitly upon the path length of the charged particle beam. This behaviour can most easily be seen by substituting the Cherenkov condition into (4).

The parameter a depends on the path length L, as well as the propagation angle θ. For a small value of L, the value of a is large so that the oscillations in the frequency distribution are closely spaced and vice versa as the path length increases. In what follows this behaviour is not evident since the calculations and graphs are relative to f_0.

CHARGE DISTRIBUTION EFFECTS

As mentioned above, our emphasis has been on charge distributions with cylindrical symmetry; in particular on line charges whose only variation is along the direction of propagation, z. Most of the interesting effects may be demonstrated with this simple geometry. With that restriction, the charge distribution is

$$\rho(\mathbf{r}) = \delta(x)\,\delta(y)\,\rho_0(z) \tag{15}$$

where $\rho_0(z)$ is the charge per unit length, and in this case, the form factor becomes a function of k_z only.

$$k_z = k\cos\theta = (2\pi\nu/c)\cos\theta \tag{16}$$

Using this simplification, we give several elementary examples to show how the frequency distribution of radiation depends on the charge distribution of a single bunch and the path length of the beam.

1. ***Point Charge.*** The Fourier transform of a δ function is a uniform function, so that the form factor for a point charge is identically unity for all values of k (or ν). Consequently, the only contribution to a variation of radiation with frequency in (12) is the last factor, $\sin^2(a\nu)$. *In this case*, only the path length of the beam, and the angle of propagation affect the frequency distribution, and there is no modulation of the oscillations of the frequency distribution from the form factor. The behaviour of the $\sin^2(a\nu)$ function was discussed in the previous section and plotted in Fig.(2). The frequency distribution for a point charge is a constant whose value depends on the viewing angle multiplied by the $\sin^2(a\nu)$ factor whose frequency depends on angle as shown in Fig.(2). The results reduce to the usual calculation of Cherenkov radiation when the wavelength is small compared to the path length, L.

2. Rectangular Line Charge. A uniform line charge of length χ has a constant charge distribution also of length χ. The form factor for this charge distribution is

$$F(k_z) = \text{sinc}\left(\frac{k_z \chi}{2}\right) \tag{17}$$

where $\text{sinc}(x) = \frac{\sin(x)}{x}$. Substituting for k_z gives R^2 as

$$R^2 = 4\,G^2\,[\sin(a\nu)\,\text{sinc}(b_1\nu)]^2 \tag{18}$$

where a is as before in (13), b_1 is given by

$$b_1 = \pi \cos\theta / f_1 \tag{19}$$

and the characteristic bunch frequency, f_1, is defined as

$$f_1 = c/\chi \tag{20}$$

For a rigid charged particle beam, the bunch length remains constant. If N_1 is the ratio of path length to bunch length, it is also the ratio of bunch to path frequency by virtue of (9) and (20).

$$N_1 = \frac{L}{\chi} = \frac{f_1}{f_0} \tag{21}$$

Then b can be expressed in terms of the path frequency

$$b_1 = \pi \cos\theta / N_1 f_0 \tag{22}$$

The frequency distribution (18) is of the type alluded to above; the oscillating $\sin^2(a\nu)$ function is modulated by $\text{sinc}^2(b_1\nu)$, the form factor characteristic of a (rectangular) charge distribution.

Although not a periodic function, $\text{sinc}^2(b_1\nu)$, the form factor part of (18), has zeroes with an equal spacing of

$$\Delta\nu_1 = f_1 \sec\theta = N_1 f_0 \sec\theta \tag{23}$$

The number of cycles of the oscillating $\sin^2(a\nu)$ function which fall between the zeroes of the form factor depends upon the relative size of the spacings of the frequency zeroes given by (14) and (23). Both sets are equally spaced, but with values which depend differently on the propagation angle, in addition to the path and charge dimensions. Their ratio is

also the ratio of the parameters a and b_1

$$r_1 = \frac{a}{b_1} = \frac{\Delta\nu_1}{\Delta\nu_p} = N_1 \frac{(n\beta)^{-1} - \cos\theta}{\cos\theta} \tag{24}$$

Just as in an optical diffraction pattern, there are (r_1-1) zeroes of the oscillating $\sin^2(a\nu)$ function between the zeroes of the $\mathrm{sinc}^2(b_1\nu)$ modulating function. Furthermore, (24) shows that the details of the frequency distribution depend on the propagation angle, the energy (through $n\beta$), and the relative dimensions of the path and charge.

The angular portion of (24) is r_1/N_1 . Fig.(3) shows a plot of the angular portion of (24) calculated for $n\beta = 1.1$, and for $n\beta = 0.9$. The behaviour in both regimes is similar. The functions have small values at small angles with respect to the forward direction, a singularity at 90 degrees, and decreasing values in the back direction ($\theta > 90$) but larger than in the forward direction. The two regimes differ in the forward direction where the function for the Cherenkov regime is negative at angles less than the Cherenkov angle. For considerations of power or energy, the sign of the functions is unimportant. In order to display $\Delta\nu_1/\Delta\nu_p$, Fig.(3) must be multiplied by the ratio N_1. The difference between a plot of (24) and Fig.(3), is only the scale factor N_1, and consequently Fig.(3) with an appropriate scale will, in principle, serve for any combination of path length and bunch length.

Figures (4) – (7) calculated for $N_1 = 10$, $n\beta = 1.1$, and various angles, show the frequency dependence of the Cherenkov radiation from a rectangular line charge. Since the square of the radiation function (12) includes the factor $G^2(n\beta,\theta)$ which becomes very small at large angles of propagation, a normalized squared radiation function is plotted.

$$R^2/4G^2 = \sin^2(a\nu)F^2(\nu) \tag{25}$$

Table I lists the values of propagation angles, and relative periods for this set of figures. For ease of understanding, the plots are presented in order of decreasing angle.

Fig.(4) calculated for the back direction of 135 degrees clearly shows the modulation of the $\sin^2(a\nu)$ oscillations by the form factor. As the propagation angle moves toward the forward direction, the frequency of the $\sin^2(a\nu)$ oscillations decreases as shown in Fig.(2), and the magnitude of the period ratio $\Delta\nu_1/\Delta\nu_p$ decreases as shown in Fig.(3) and Table I.

The result of these two effects is that there are fewer oscillations for a given frequency interval, and also there are fewer oscillations between zeroes of the modulation function. In addition, as fewer oscillations occur between the modulation zeroes, the relative signal intensity decreases since there are now fewer oscillation peaks at the at the higher valued part of the modulation curve. Thus, it becomes increasingly difficult to discern the shape and extent of the modulation as the propagation angle decreases. These effects are shown in Fig.(4)–(6).

As the propagation angle moves further forward, the null density, a/π, continues to decrease until it goes to zero at the Cherenkov angle of $\theta_c = 24.6$ degrees. Further into the forward direction the propagation angle is inside the Cherenkov cone. For propagation directions near the Cherenkov angle, there is a region where $|\Delta\nu_1/\Delta\nu_p| < 1$. In this region the spacings of the oscillations are greater than the spacings between the zeroes of the modulation function; less than one cycle of oscillation occurs for every modulation zero.

Figure (7), calculated for a propagation angle of 15 degrees, shows the frequency distribution for this situation where $\Delta\nu_1 = 10.4\ f_0$ and $\Delta\nu_p = -17.6\ f_0$. The result of this strong modulation is to greatly decrease the relative intensity of the frequency distribution, since again the oscillations have fewer opportunities to reach their full height when the modulation function is large.

The extent of the regions in which $|r_1| = |\Delta\nu_1/\Delta\nu_p| < 1$ can be investigated by a further consideration of Fig.(3). As noted above, N_1 is the scale factor for the ordinate in order to make the figure apply to a particular value of L/χ, i.e. to make the figure a plot of (24). Then the angular values for which $|r_1| < 1$ are given by those parts of the curve lying between $r_1 = +1$ and $r_1 = -1$.

In the Cherenkov regime the graph of (24) passes through zero at the Cherenkov angle, and therefore, there is always a region near θ_c where $|r_1| < 1$. The bounds of this region depend on the scale factor N_1. As N_1 increases, the curve for $\Delta\nu_{b1}/\Delta\nu_p$ becomes steeper, it intersects the limit lines $r_1 = +1$ and $r_1 = -1$ more nearly at a right angle, and the region decreases in angular extent. Whether or not the region reaches to $\theta = 0$ also depends on the value of N_1. If N_1 is larger than$((1/n\beta) - 1)^{-1}$, the part of the curve near zero will extend beyond $r_1 = -1$ and the region will be limited.

At $\theta = \pi$ the value of Fig.(3) is $-((1/n\beta) + 1)$ which is approximately -2 for values of $n\beta$ near 1. Thus it can be seen that for values of N_1 sufficiently smaller than one, it is possible to have an intersection of the $\Delta\nu_1/\Delta\nu_p$ curve with the $r_1 = -1$ limit line. This situation demands a small value for N_1 whereas the limit near $\theta = 0$ reqires a large value. Consequently the two are mutually exclusive; only one can occur for a given value of N_1. For values of N_1 between the large and the small limiting cases, neither of these intersections with the $r_1 = -1$ limit will occur.

Thus in the Cherenkov regime, there is always an angular region near θ_c where the modulation period is greater than the oscillation period, and if the path length is large compared to the bunch length, the region is bounded by an angle greater than zero. If the bunch length is larger than the path length, the forward region of small r extends to $\theta = 0$ and there may exist another such region in the back directions. Behaviour in the sub–Cherenkov regime is exactly the same except that the forward region of small r_1 always extends to $\theta = 0$. Table II shows the limits of the regions for both regimes.

3. Triangular Line Charge. The form factor for a triangular charge distribution with a base length of d is

$$F(k_z) = \text{sinc}\left(\frac{k_z d}{4}\right) \tag{26}$$

To consider other than a uniform line charge distribution it is convenient to use the average length as a comparison basis. For a uniform charge distribution of length χ, the average length *is* the charge length χ. For a line charge whose charge density varies in a triangular fashion over the base length d, the average length is one half the base length,

$$\chi = \frac{d}{2} \tag{27}$$

Using this value, the form factor for a triangular line charge is the square of the form factor for a rectangular line charge.

$$F(k_z) = \left\{ \text{sinc}\left(\frac{k_z \chi}{2}\right) \right\}^2 \tag{28}$$

Substituting for k_z gives R^2 as

$$R^2 = 4\, G^2 \left[\sin(a\nu) \left\{ \text{sinc}(b_1\nu) \right\}^2 \right]^2 \tag{29}$$

where a is given by (13), and using the average length as defined by (27), and b_1 is given by (22) as in the case for the rectangular charge distribution.

The frequency distribution for triangular charge bunch is similar to that of the rectangular one except that the sinc function is raised to the fourth power instead of the second. This means that the modulation of the oscillations decreases in value much more rapidly than for the rectangular charge bunch.

Fig.(8) shows the normalized frequency distribution calculated for $n\beta = 1.1$, $N_1 = 10$, and an angle of $\theta = 60$ degrees. Comparison with Fig.(5), calculated using the same values for a rectangular charge distribution, shows that the frequency distribution for a triangular charge decreases much off more rapidly. The frequency distributions for other angles of propagation behave similarly. Furthermore, in terms of the average length, the discussion of the region of high modulation (where $|r_1| < 1$) is identical to that for the rectangular charge distribution.

4. Trapezoidal Line Charge. A symmetric trapezoidal charge distribution is characterized by two lengths; the base length, d_1, and the length of the top, d_2. The Fourier transform of this shape is best expressed in terms of the average length

$$\chi = \frac{d_1 + d_2}{2} \tag{30}$$

and the rise distance

$$\delta = \frac{d_1 - d_2}{2} \tag{31}$$

Using these definitions, the form factor is

$$F(k_z) = \text{sinc}(\frac{k_z \chi}{2}) \text{ sinc}(\frac{k_z \delta}{2}) \tag{32}$$

The two characteristic lengths each have an associated frequency. The bunch frequency continues to be defined by (20), while the new rise distance frequency is

$$f_2 = c/\delta \tag{33}$$

Substituting for k_z, as before, gives the square of the radiation function

$$R^2 = 4\ G^2 [\sin(a\nu)\ \text{sinc}(b_1\nu)\ \text{sinc}(b_2\nu)]^2 \tag{34}$$

where, a is as before, b_1 is given by (19), and b_2 is

$$b_2 = \pi \cos\theta / f_2 \tag{35}$$

Continuing to assume a rigid beam so that the the lengths χ and δ remain constant, their ratio is

$$N_2 = \chi / \delta = f_2 / f_1 \tag{36}$$

and the ratio of path length to average bunch length,as given by (21), is unaffected. For a trapezoid, $d_1 > d_2$, and thus $\chi > \delta$, so that $N_2 > 1$.

For a rigid beam, b_1 can be expressed in terms of the path frequency as in (22)

$$b_1 = \pi \cos\theta / N_1 f_0 \tag{22}$$

and b_2 can be written in terms of b_1.

$$b_2 = b_1 / N_2 \tag{37}$$

For this case, the frequency distribution is the familiar $\sin^2(a\nu)$ function now modulated by the product of the squares of two sinc functions; the one containing b_1

depends on the ratio of path length to bunch length, the one with b_2 depends on the ratio of path length to rise distance. The resulting radiation function is similar to those above, but more complicated, because two parameters, χ and δ are invovlved.

The ratio of the zero spacings of the bunch average length modulation to those of the path length oscillations is given by (24). The ratio of the zero spacings of the bunch rise distance modulation to those of the path length oscillations is (24) multiplied by N_2.

$$r_2 = \frac{\Delta \nu_2}{\Delta \nu_p} = N_2 r_1 = N_2 N_1 \frac{(n\beta)^{-1} - \cos \theta}{\cos \theta} \qquad (38)$$

As a result of its steep ends, a rectangular charge bunch has a frequency distribution which is relatively large at high frequencies. Other distributions which have less abrupt changes in the charge density have a smaller high frequency component. For these other distributions, it is difficult to display the higher frequency portions of the distribution on a linear intensity scale, as is evidenced in Fig.(8) for the triangular charge bunch. A logarithmic scale is more appropriate. Figures (9)–(11) show the frequency distributions for the rectangular, triangular, and trapezoidal charge distributions, all calculated for the same angle of propagation, 60 degrees.

In these figures, carried out to 100 f_0, the zeroes of the path length oscillations are 2.44 f_0 apart, the average length modulation has zeroes with 20 f_0 spacing and the rise distance modulation has a spacing of 50 f_0. The resulting differences in the graphs is clearly evident at the higher harmonics. It is necessary to carry the calculations to such a high harmonic of the path frequency in order to show the differences; there are very small differences in the frequency distributions out to approximately the 20 harmonic.

DISCUSSION

The results of this paper are expressed by (12), along with the specific forms for the form factors given, respectively by (17), (26), and (32) for the rectangular, triangular, and trapezoidal charge distributions. Radiation given off at a particular angle has an oscillating distribution in frequency which is modulated by the frequency distribution corresponding to the shape of the charge of an individual bunch. These effects are clearly seen in Figures (4)–(11). The null density ('frequency') of the oscillations depends on the velocity of the beam, the angle of propagation of the radiation, the velocity of radiation in the medium, and on the path length of the beam, as expressed in (13).

Since the modulation of the oscillations is the fourier transform of the charge distribution, the results are similar to those found in fourier optics for intensity distributions of diffraction from apertures of the same shape. The spatial envelope given by $G^2(n\beta,\theta)$ has a maximum in the sub–Chernkov regime, and is highly peaked in the neighborhood of the Cherenkov angle in the Cherenkok regime.. Consequently the intensity of radiation is quite small away from the peak, in the backward or extreme forward direction. In order to clearly display the effects of beam length, and bunch length and shape, Figures (4)–(11) show only the square of the normalized radiation function, $R^2/4G^2$.

Several simple examples are given, with the rectangular charge bunch discussed in detail in order to show how the results depend on the propagation angle We note that the triangular and rectangular shapes are the two limits of the trapezoidal shaped charge distribution and that the transition from one to the other is continuous so that the detailed discussion of the angular effects also applies to the triangular and trapezoidal distributions. A discussion of other shapes is possible, but not necessary.

There are several special angles at which the above analysis is modified. At the Cherenkov angle, the value of a as given by (13) is zero and there is no oscillation in frequency of the radiation. In this case, the radiation from all sources along the path of the beam arrive at the observer simultaneously in an electromagnetic shock front. The intensity of this front is finite as mentioned in reference 5.

At a propagation angle of 90 degrees the form factor for any one dimensional charge shape is identically one, so that there is no modulation of the frequency distribution. Such a case would lead to an amount of radiation which is unbounded at high frequencies except that dispersion causes the index of refraction to become less than unity at high frequencies. At other angles the radiation diminshes at high frequencies because the form factor always decreases as its argument becomes large.

An implicit assumption in this analysis is that although power is lost through radiation by the charged particle beam, the resulting slowing of beam along its flight path is negligible. For a relativistic beam, large changes in energy yield only small changes in β which is the important parameter here. As seen from (3) the intensity of the coherent Cherenkov radiation is proportional to the square of the charge of an individual bunch. Thus, at high beam current, coherent Cherenkov radiation is expected to be a dominant loss mechanism, and the energy of the beam may change significantly along its length.

Additionally, the index of refraction is assumed constant. It is well known that dispersion causes the index to change with frequency, and it may also be affected by plasma heating of the medium in the vicinity of the beam. The beam is also assumed to be rigid, *i.e.* an individual bunch retains its charge and shape as it traverses the path. If the beam radiates strongly, or has a relatively large emittance, the bunches may not be rigid. A more detailed analysis would address these considerations.

This analysis could be used as a diagnostic for a charged particle beam. In order to distinguish between various charge shapes, it would be necessary to receive signals over an

extended frequency range as mentioned in discussing Fig. (9–11). Such measurements could be accomplished using log–periodic antennas or wide band TEM horns. This discussion assumes that the RF signals propagate unimpeded. In real experiments, reflections from the surrounding environment must be taken into account

Finally, we note that it is possible to measure the radiated electric field rather than power. In this case, the comparison of such measurements should be to the radiation function, not its square, so that the phase must be considered. The minus signs ignored here then would become meaningful.

ACKNOWLEDGEMENT

This work was supported by the Defense Advanced Research Projects Agency, and the Space and Naval Warfare Systems Command under the Naval Postgraduate School Direct Funded Research Program.

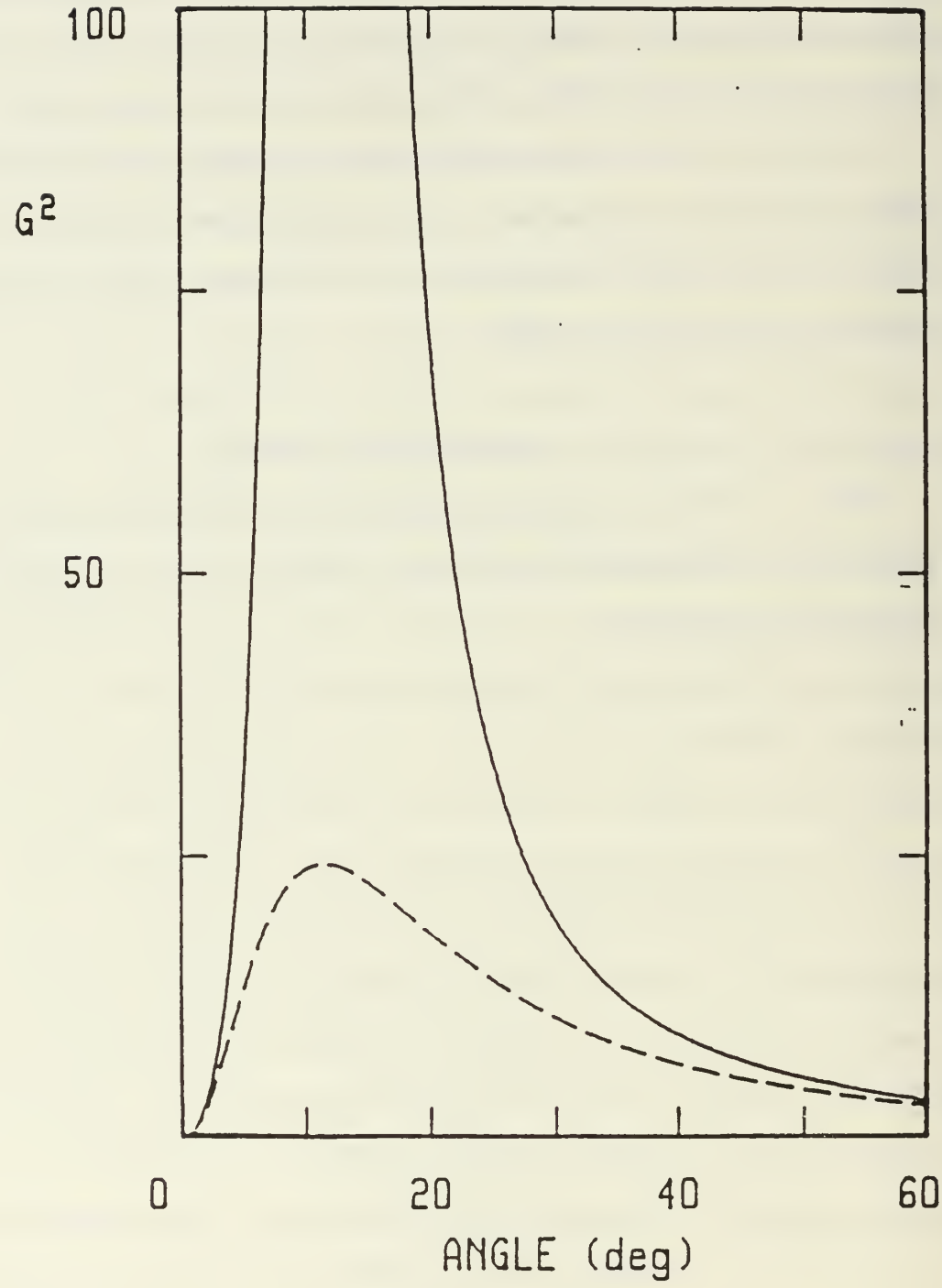

Figure1. Envelope function $[G(n\beta,\Theta)]^2$ as a function of angle. The solid line (Cherenkov) is for $n\beta = 1.02$. The dashed curve (Sub–Cherenkov) is for $n\beta = 0.98$. From Reference 5.

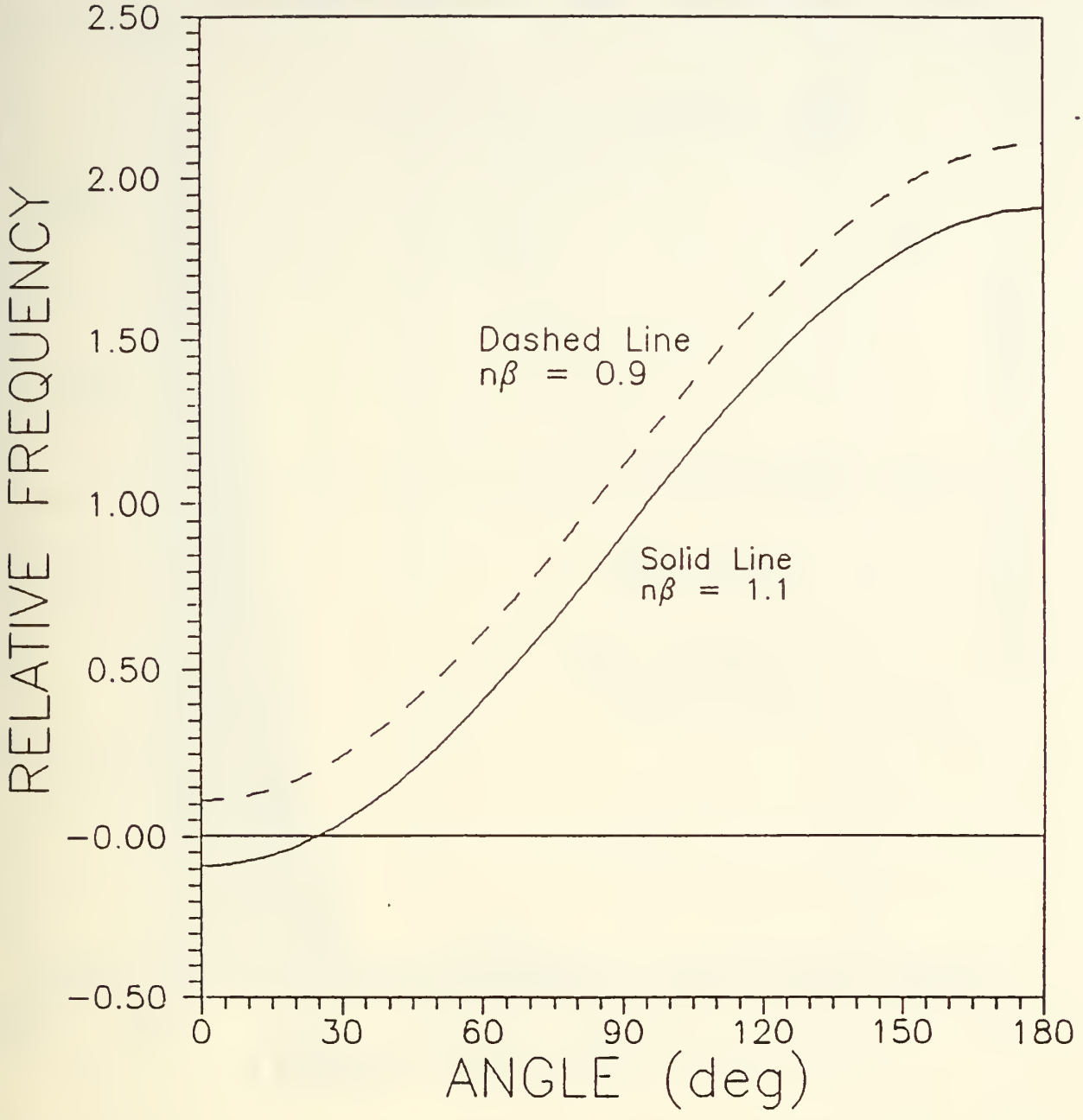

Figure2. Graph of Equation (14A), the normalized null density as a function of angle of propagation with respect to the beam line. Here f_0 is the path frequency and Δv_p is the spacing of zeros in the oscillations of the frequency distribution.

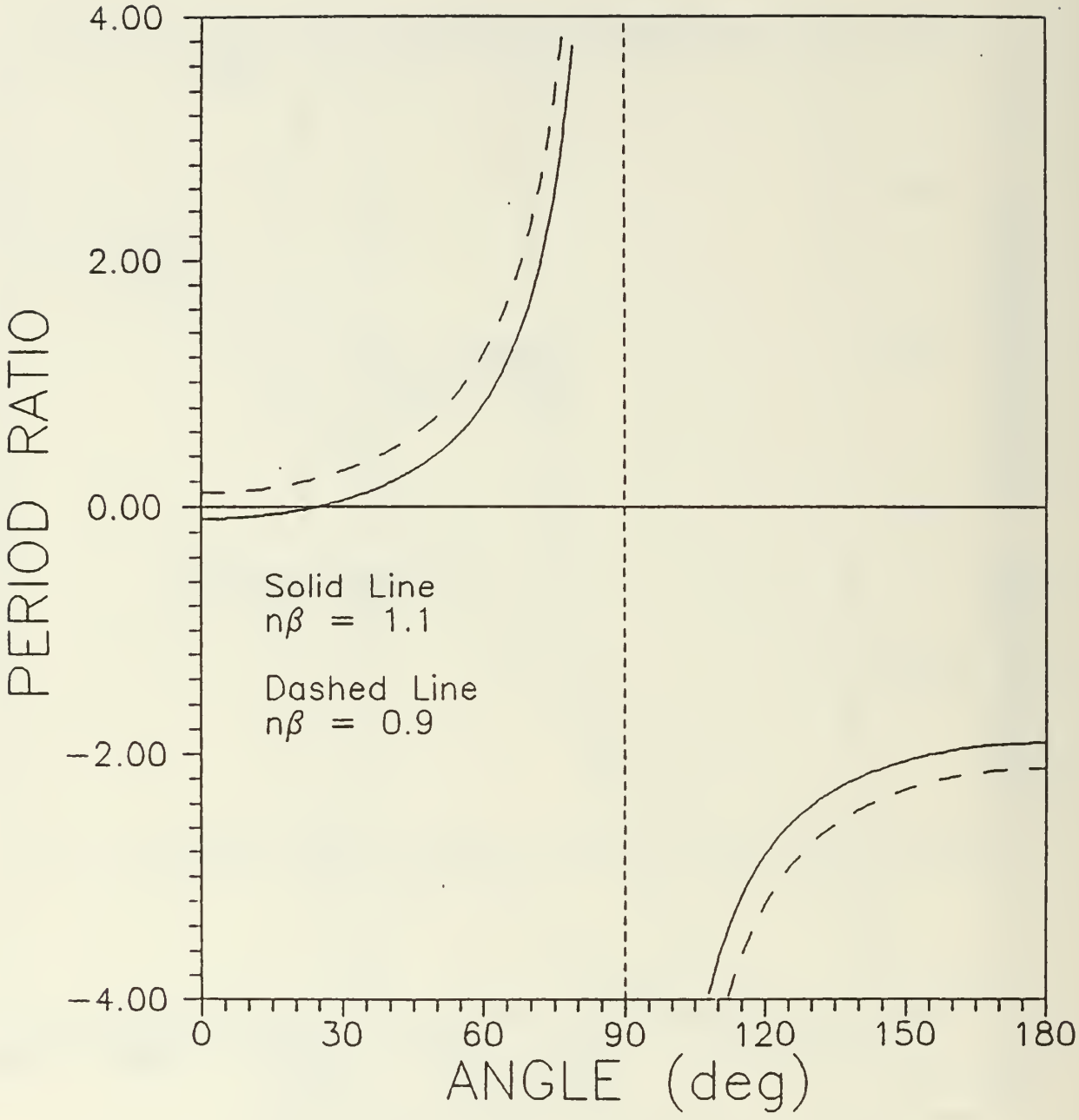

Figure3. Graph for rectangular charge distribution of the ratio of the spacing of zeros in the frequency distribution resulting from the bunch length to those resulting from the path length plotted as a function of angle with respect to the beam line. This is a plot of the angular portion of Equation (24), i.e. r_1/N_1 as a function of angle.

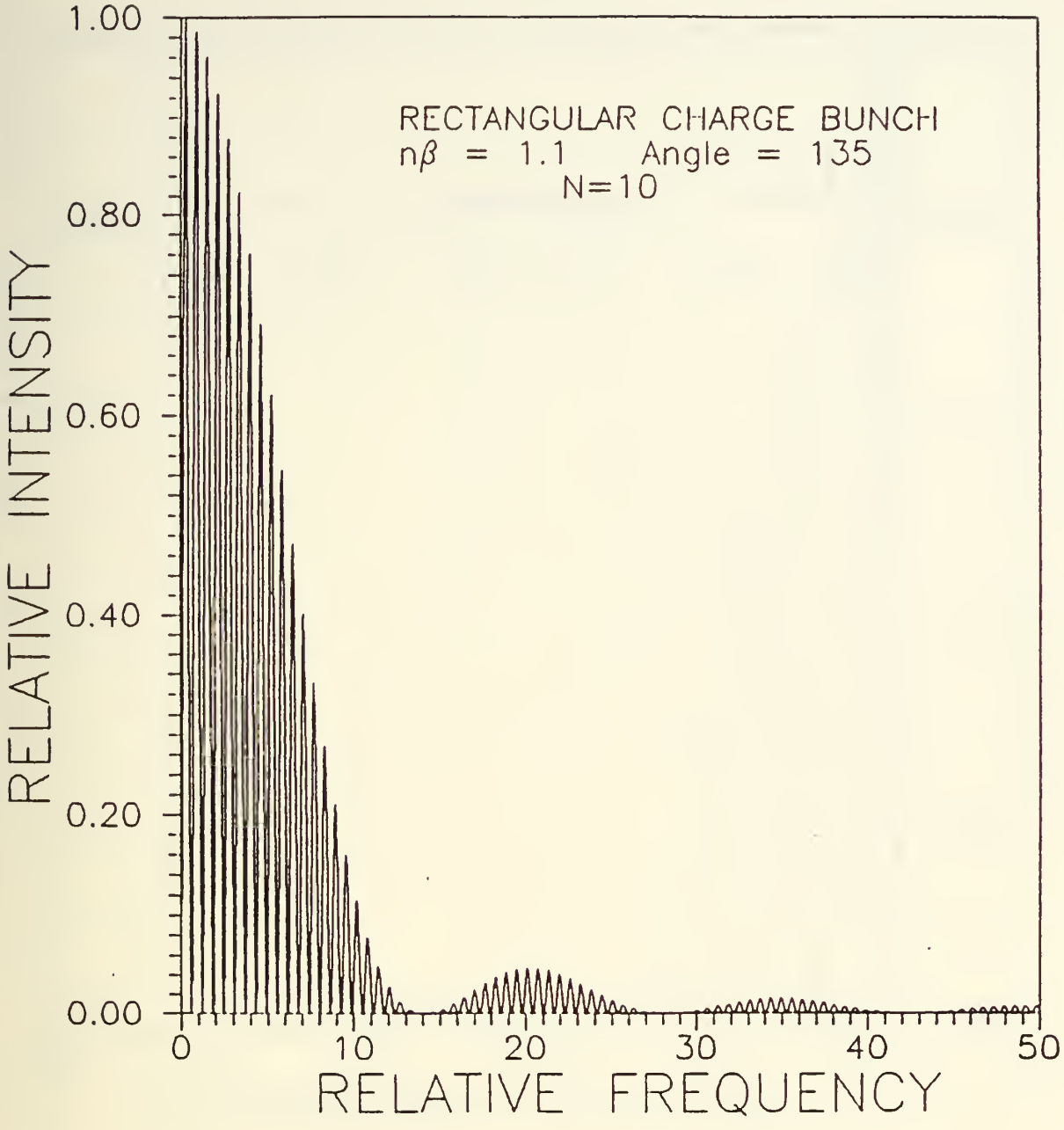

Figure4. Scaled frequency dependence of Cherenkov radiation from a beam composed of ten rectangular charge bunches for propagation at an angle of 135 degrees with respect to the beam path.

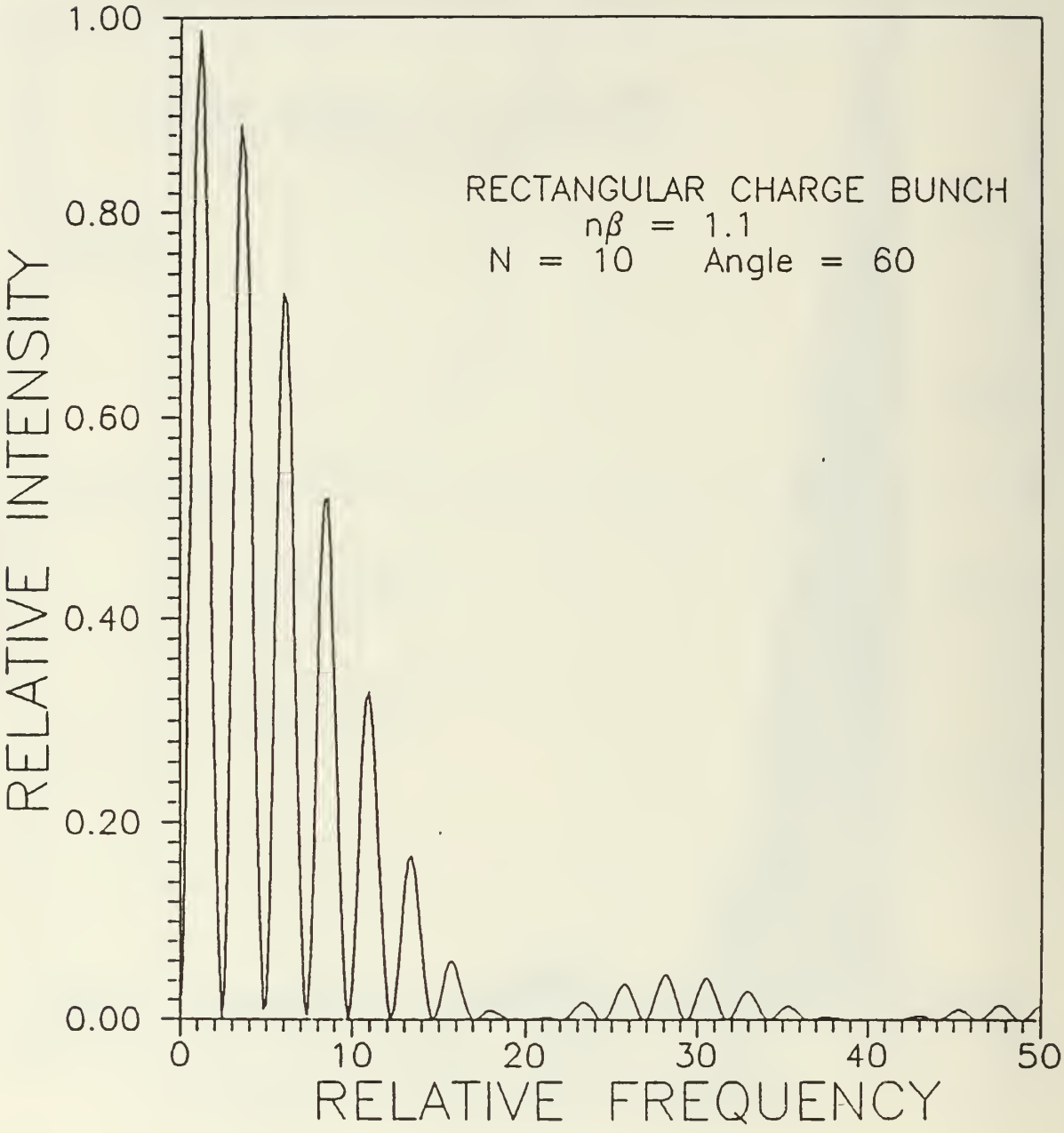

Figure5. Scaled frequency dependence of Cherenkov radiation from a beam composed of ten rectangular charge bunches for propagation at an angle of 60 degrees with respect to the beam path.

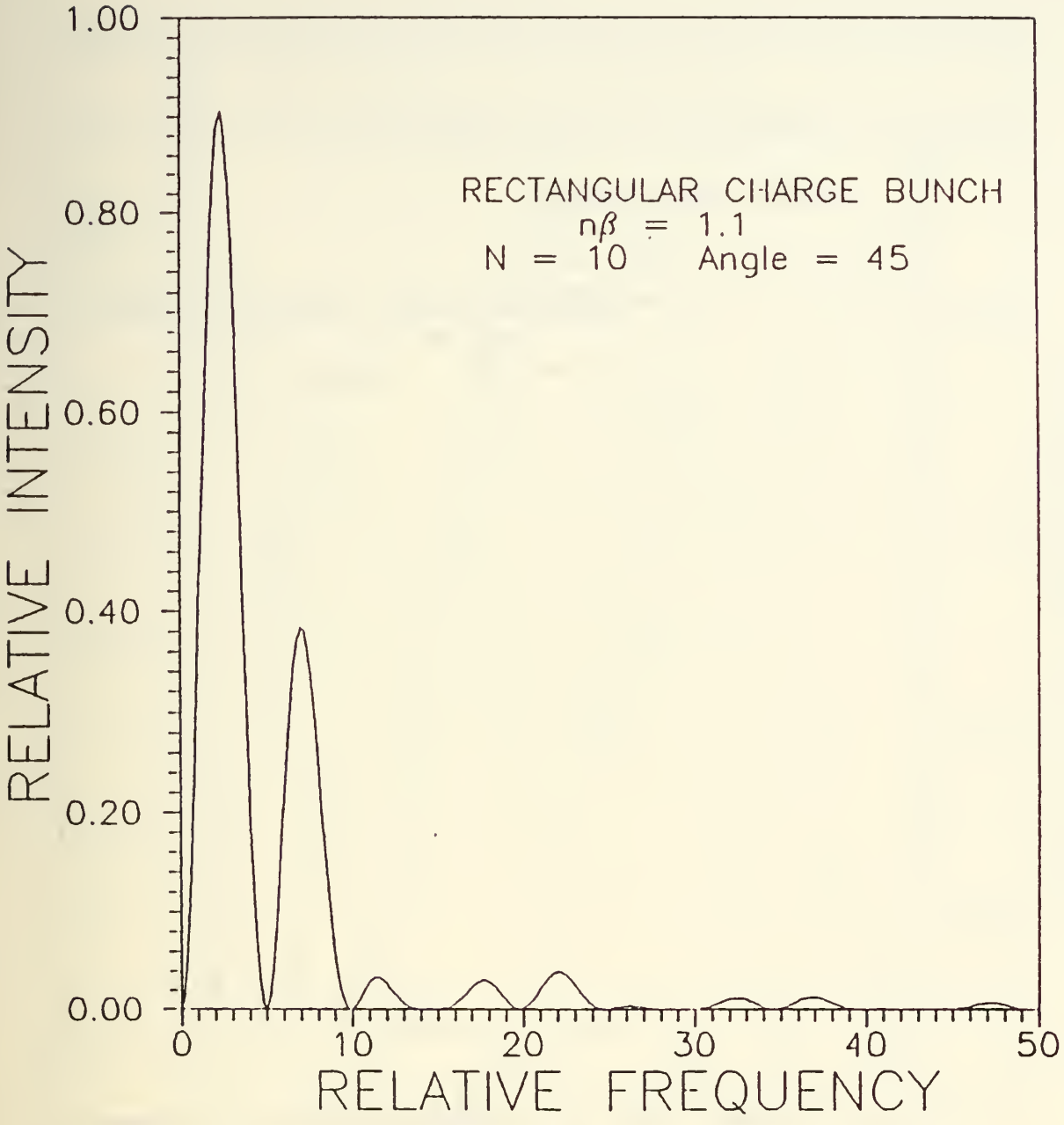

Figure6. Scaled frequency dependence of Cherenkov radiation from a beam composed of ten rectangular charge bunches for propagation at an angle of 45 degrees with respect to the beam path.

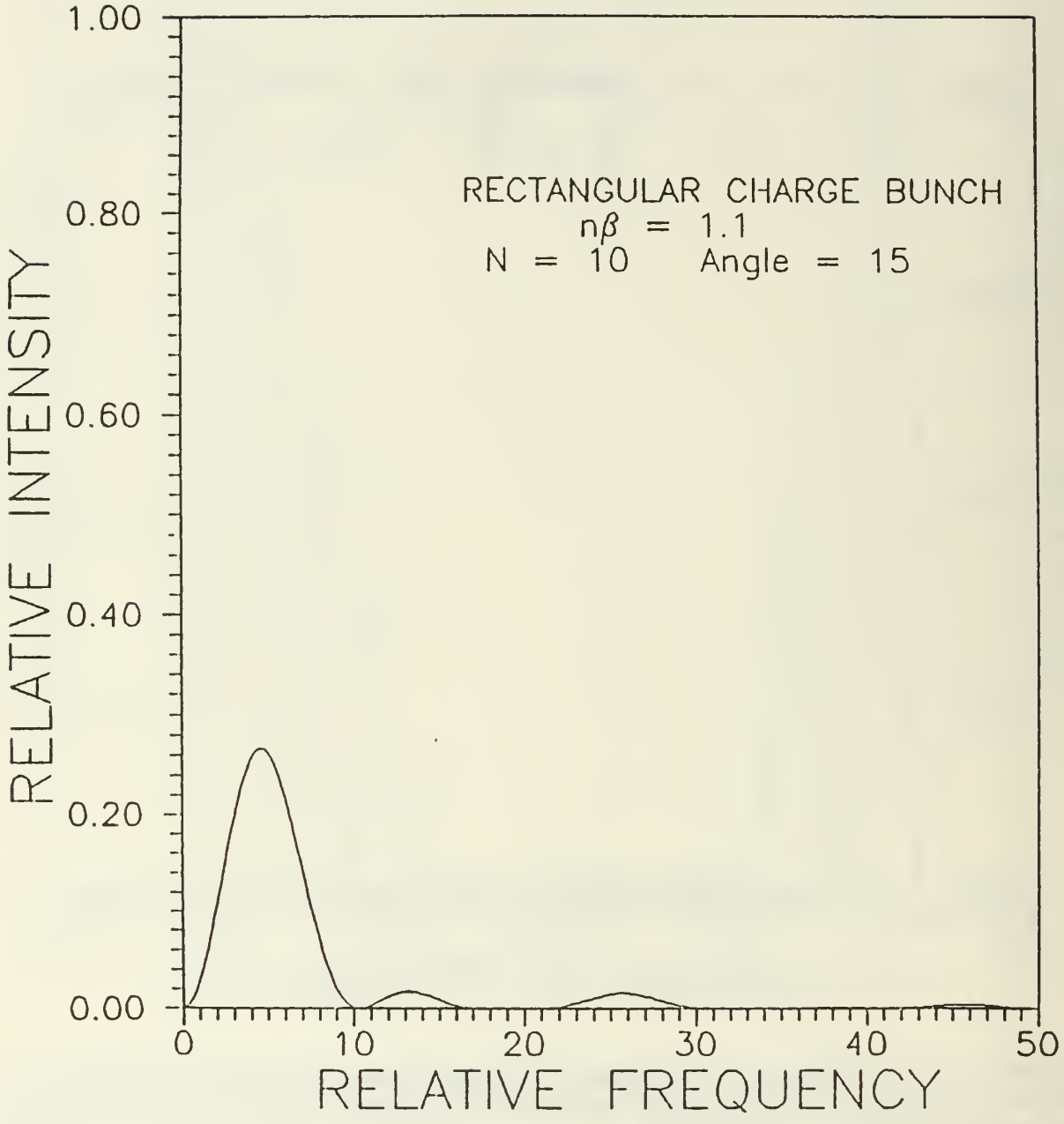

Figure7. Scaled frequency dependence of Cherenkov radiation from a beam composed of ten rectangular charge bunches for propagation at an angle of 15 degrees with respect to the beam path.

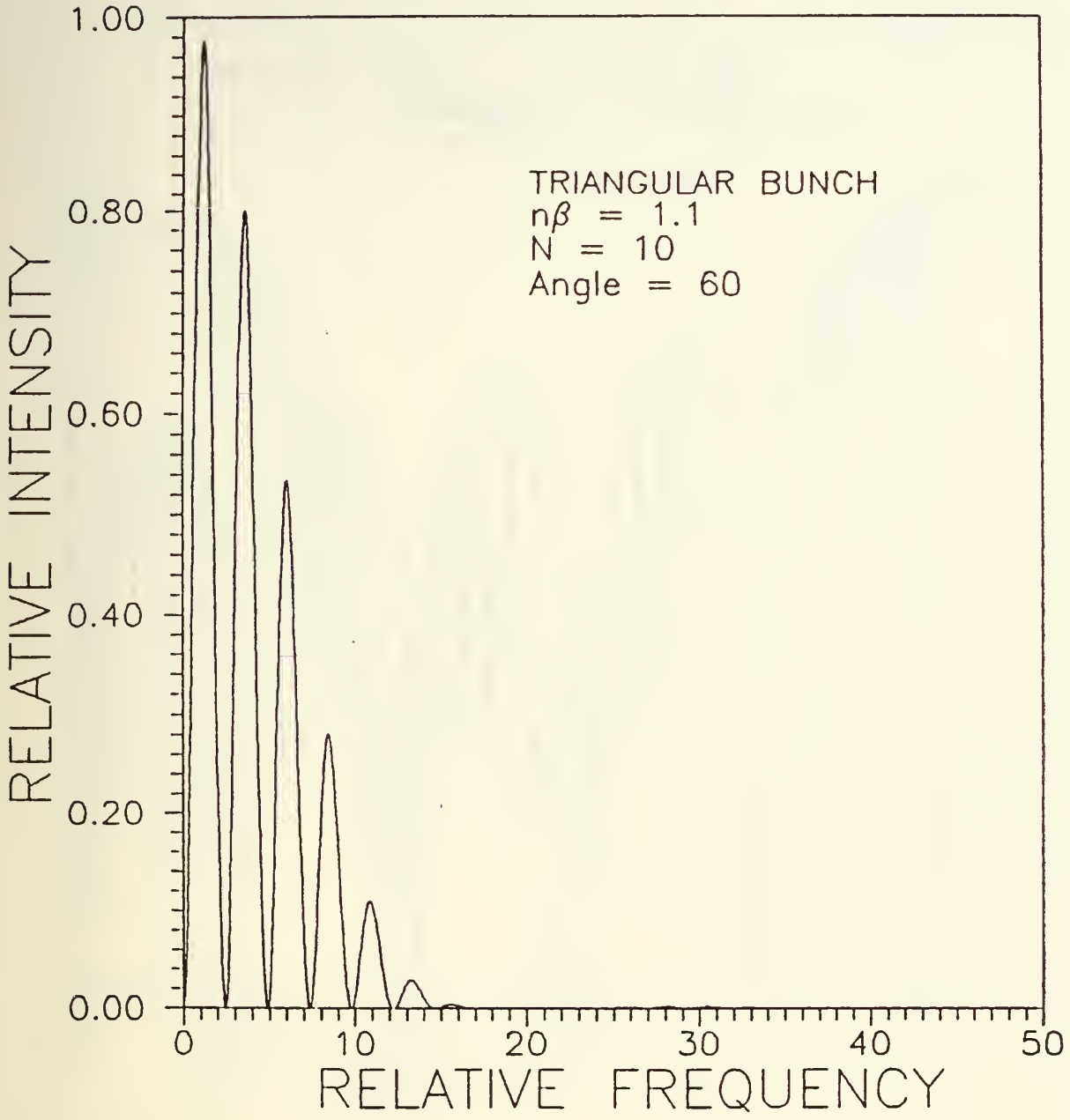

Figure8. Scaled frequency dependence of Cherenkov radiation from a beam composed of ten triangular charge bunches for propagation at an angle of 60 degrees with respect to the beam path.

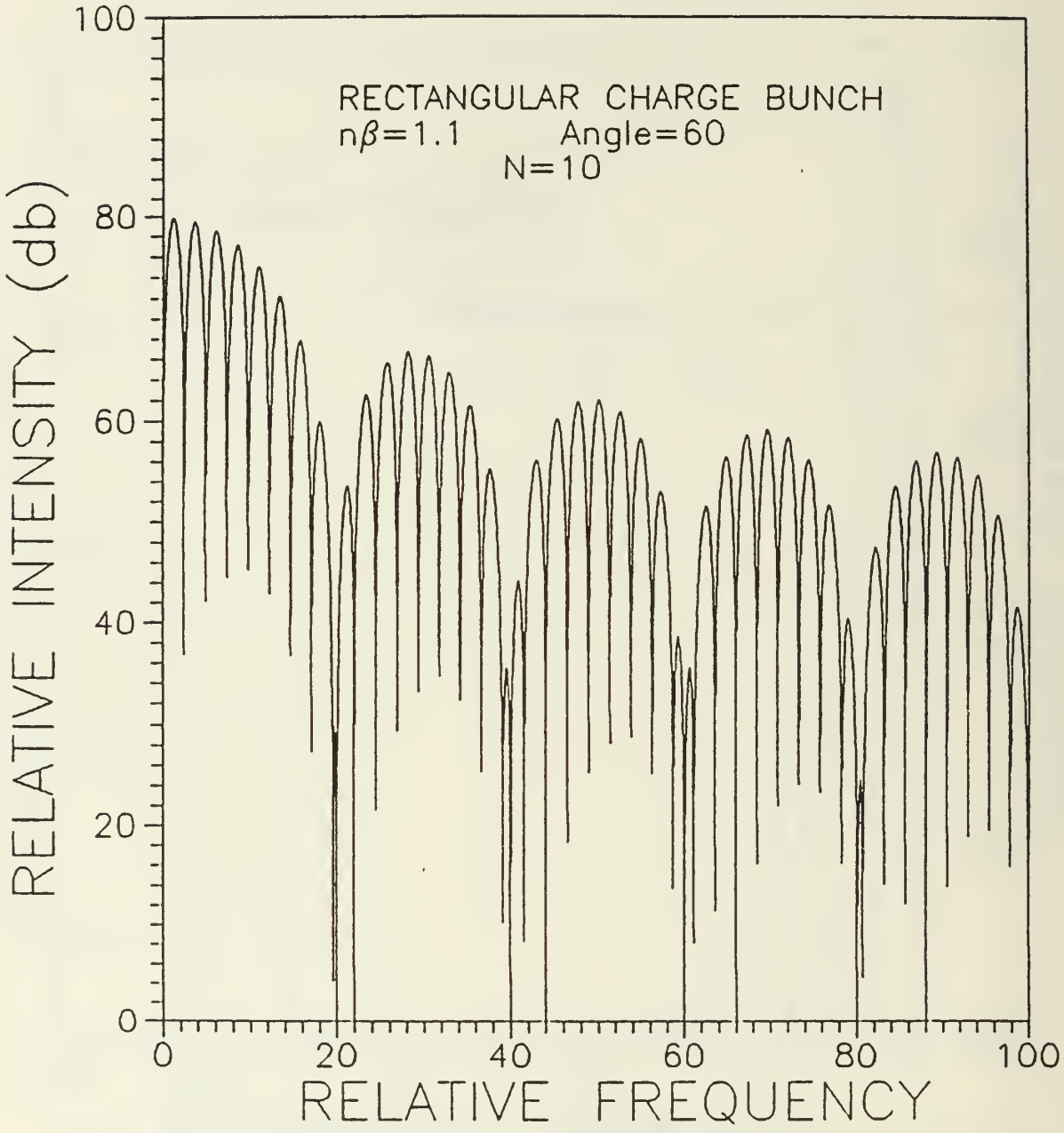

Figure9. Relative intensity (db) of the scaled frequency dependence of Cherenkov radiation from a beam composed of ten rectangular charge bunches for propagation at an angle of 60 degrees with respect to the beam path. The reference level is $I_0 = 10^{-8}$.

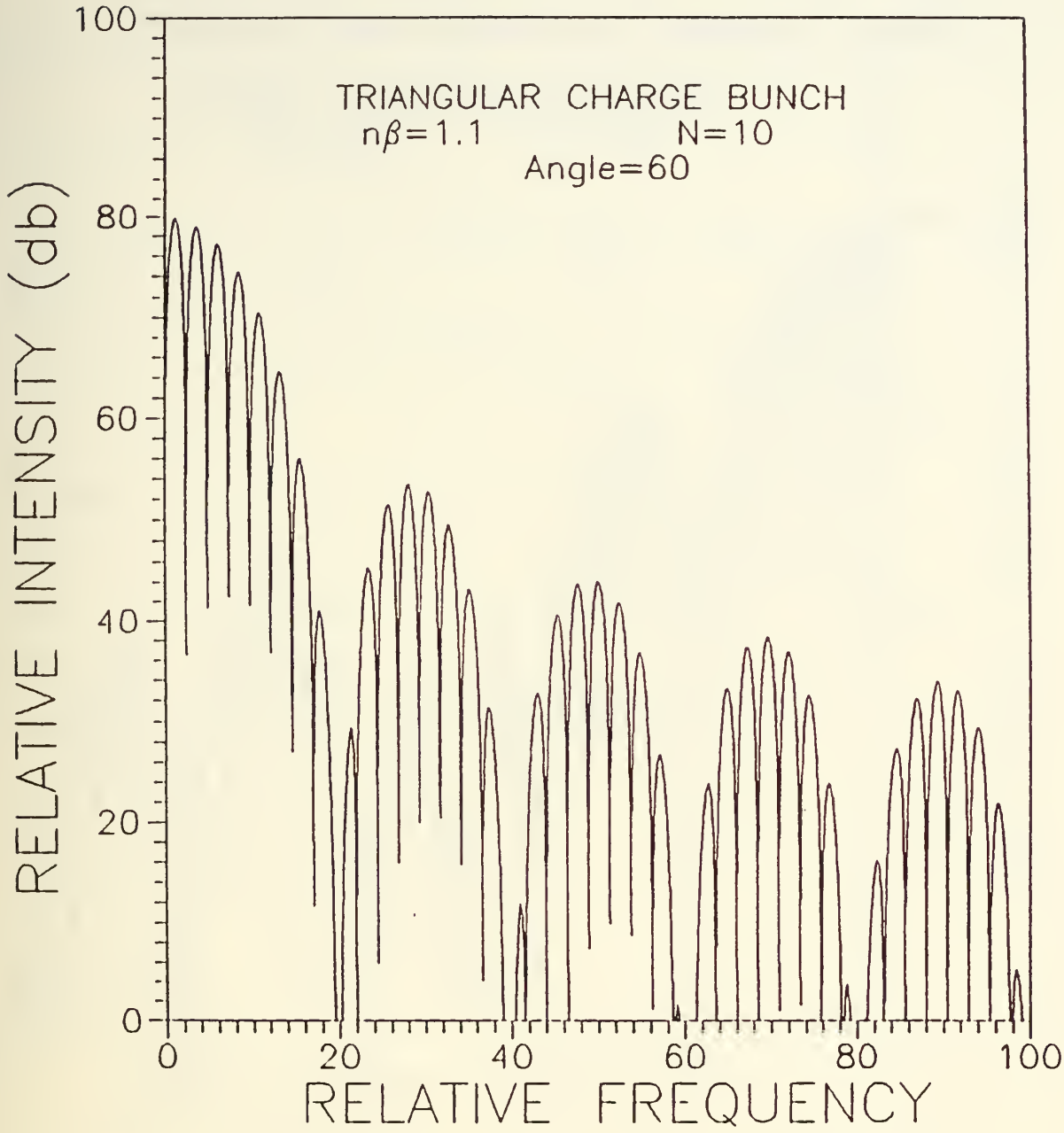

Figure10. Relative intensity (db) of the scaled frequency dependence of Cherenkov radiation from a beam composed of ten triangular charge bunches for propagation at an angle of 60 degrees with respect to the beam path. The reference level is $I_0 = 10^{-8}$.

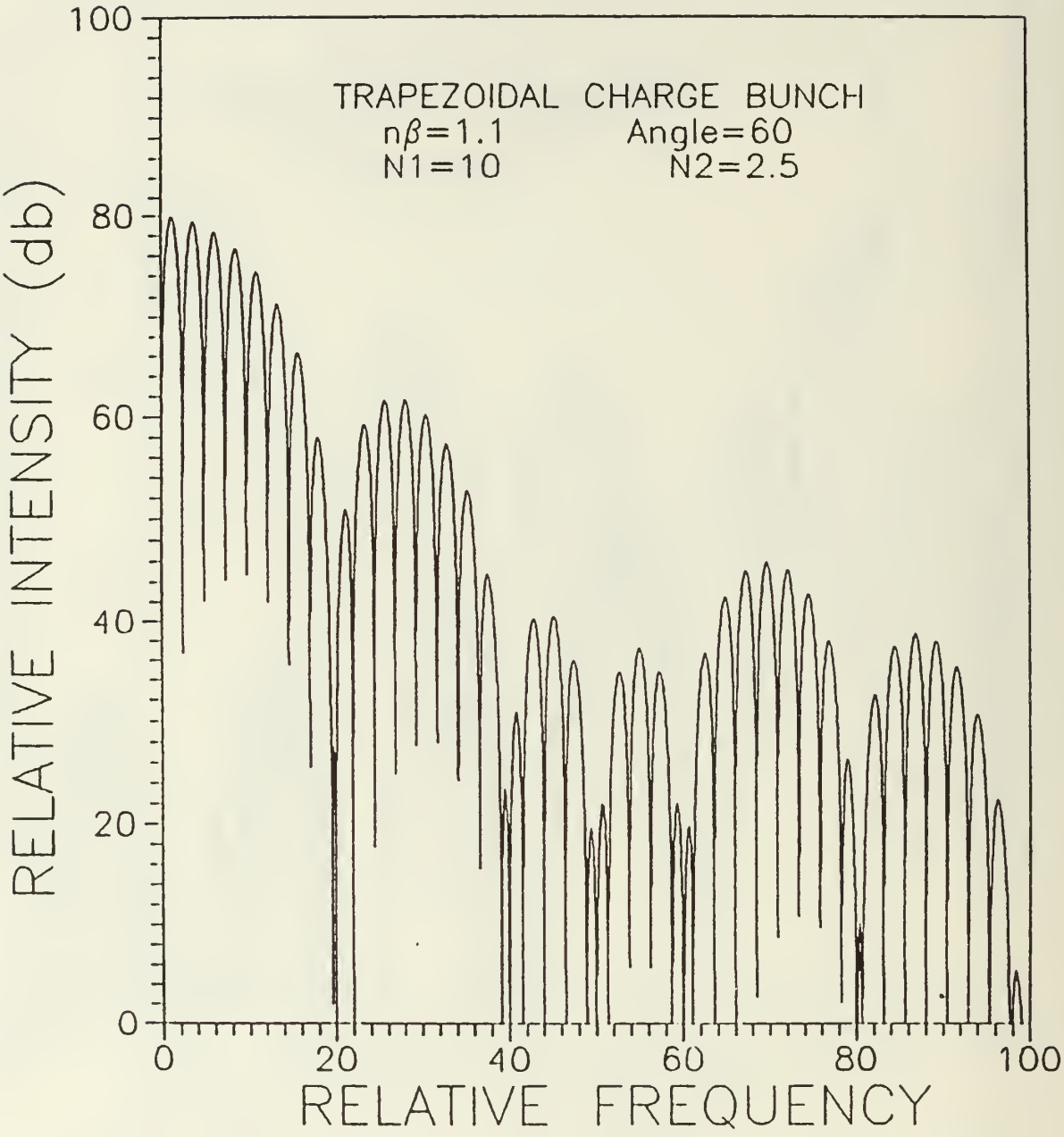

Figure11. Relative intensity (db) of the scaled frequency dependence of Cherenkov radiation from a beam composed of ten trapezoidal charge bunches for propagation at an angle of 60 degrees with respect to the beam path. The reference level is $I_0 = 10^{-8}$.

TABLE I

Propagation angles and period ratios for a rectangular charge bunch.

Calculated for $r_1 = 10$ and $n\beta = 1.1$.

Angle	$\frac{\Delta \nu_p}{f_0}$	$\frac{\Delta \nu_1}{f_0}$	$\frac{\Delta \nu_1}{\Delta \nu_p}$
0	–11.0	10.0	–0.909
15	–17.6	10.4	–0.59
$\theta_c = 24.6$		—	0
45	4.95	14.1	2.86
60	2.44	20.0	8.18
135	0.619	14.1	–22.9
180	0.524	–10.0	–19.1

Table II

Bounding angles and conditions under which $\frac{\Delta v_1}{\Delta v_p} \leq 1$. The ratio of beam path length to bunch length is $N_1 = \frac{L}{\chi}$. The Chevenkov angle is $\Theta_c = \text{Cos}^{-1}(\frac{1}{n\beta})$.

Bounding Angle	Radiation Regime	Angular Range	Conditions on N_1
$\text{Cos}\Theta_a = \frac{1}{n\beta}\frac{N_1}{N_1 - 1}$	$n\beta > 1$	$0 < \Theta_a < \Theta_c$	$N_1 > \frac{n\beta}{n\beta - 1}$
	All	$\frac{\pi}{2} < \Theta_a < \pi$	$N_1 < \frac{n\beta}{n\beta + 1}$
$\text{Cos}\Theta_b = \frac{1}{n\beta}\frac{N_1}{N_1 + 1}$	$n\beta > 1$	$\Theta_c < \Theta_b < \frac{\pi}{c}$	None
	$n\beta < 1$	$0 < \Theta_b < \frac{\pi}{2}$	$N_1 < \frac{n\beta}{1 - n\beta}$

In the Cherenkov regime, there is no value for Θ_a if $\frac{n\beta}{n\beta+1} < N_1 < \frac{n\beta}{n\beta-1}$.

REFERENCES

1. "Cerenkov Radiation from Periodic Electron Bunches", Fred R. Buskirk and J. R. Neighbours, Phys. Rev. A., 28, 1531 (1983)

2. "Cerenkov Radiation from a Finite Length Path in a Gas", John R. Neighbours, Fred R. Buskirk, and A. Saglam, Phys. Rev. A., 29, 3246 (1984)

3. "Observation of Microwave Cerenkov Radiation as a Diffraction Pattern", X.K. Maruyama, J.R. Neighbours, F.R. Buskirk, D.D. Snyder, M. Vujaklija and R.G. Bruce, J. Appl. Phys. 60, 518 (1986)

4. "Cerenkov Radiation and Electromagnetic Pulse Produced by Electron Beams Traversing a Finite Path in Air", Fred R. Buskirk and John R. Neighbours, Phys. Rev. A. 34, 3470 (1986)

5. "Cerenkov and Sub–Cerenkov Radiation from a Charged Particle Beam", John R. Neighbours, Fred R. Buskirk and Xavier K. Maruyama, J. Appl. Phys. 61, 2741 (1987)

6. "Microwave Cherenkov Radiation as a Diffraction Phenomenon", Xavier K. Maruyama, F. R. Buskirk and J. R. Neighbours, Nucl. Inst. and Methods in Phys. Res. B24/25 921 (1987)

7. "Effects at Resistive Loading of TEM Horns", Motoshita Kanda, IEEE Trans EM Compatibility, EMC–24, 245–255 (1982)

DISTRIBUTION LIST

LT. W. Fritchie — 1
PMW 145
SPAWAR
Washington D.C. 20363–5100

Dr. Richard Briggs — 2
L–321
Lawrence Livermore national Laboratory
Box 808
Livermore, CA 93943

The Charles Stark Draper Laboratory — 1
ATTN: Dr. Edwin Olsson
555 Technology Square
Cambridge, MA 02139

Defense Advanced Research Project Agency — 1
ATTN: LT COL George P. Lasche
1400 Wilson Blvd.
Arlington, VA 22209

Defense Advanced Research Projects Agency — 1
ATTN: Dr. Shen Shey
Directed Energy Office
1400 Wilson Boulevard
Arlington, VA 22209–2308

Defense Technical Information Center — 1
Cameron Station
Alexandria, VA 22314

Directed Technologies — 2
ATTN: Mr. Ira F. Kuhn, Jr.
Dr. Nancy J. Chesser
1226 Potomac School Road
McLean, VA 22101

Dr. V.L. Granatstein
Electrical Engineering Dept.
University of Maryland
College Park, MD 20742 — 1

Dr. C.M. Huddleston
Booz–Allen & Hamilton Inc.
4330 East West Highway
Bethesda, MD 20814 — 1

Lawrence Berkeley Laboratory
ATTN: Dr. Edward P. Lee
Building 47, Room 111
1 Cycltron Road
Berkeley, CA 94720 — 1

Lawrence Livermore National Laboratory
University of California
ATTN: Dr. William A. Barletta
Dr. Simon S. Yu
Dr. John T. Weir
Dr. Thomas J. Karr
Dr. William M. Fawley
Dr. Eugene J. Lauer
Dr. George J. Caporaso
Ms. Lois Barber
P.O. Box 808
Livermore, CA 94550 — 8

Library
Code 0142
Naval Postgraduate School
Monterey, CA 93943 — 2

Lockheed Missile and Space Co., Inc.
ATTN: Dr. John Siambis
P.O. Box 3504
Sunnyvale, CA 94088–3504 — 1

Los Alamos National Laboratory 3
ATTN: Dr. Randolph Carlson
Dr. D.C. Moir
Ms. Leah Baker
Mail Stop P942
P.O. Box 1663
Los Alamos, NM 87545

Dr. Joseph Mack 1
P4, M.S. E–554
Los Alamos National Laboratory
Los Alamos, NM 87545

Dr. Timothy Neal 1
M4 M.S.–P–940
Los Alamos National Laboratory
Los Alamos, NM 87545

Prof. T.C. Marshall 1
Dept. of Applied Physics and
Nuclear Engineering
Columbia University
New York, NY 10027

McDonnell–Douglas Corp. 1
ATTN: Dr. J. Carl Leader
P.O. Box 516
St. Louis, MO 63166

Dr. David Merritt 1
PMS 405
Strategic Systems Project Office
Naval Sea Systems Command
Washington, D.C. 20376

Mission Research Corporation 1
ATTN: Dr. N.J. Carron
P.O. Box 719
Santa Barbara, CA 93102

Mission Research Corporation — 3
Attn: Dr. Larry Wright
Dr. Barry Newberger
Dr. Dushan Mitrovitch
Plasma Sciences Division
1720 Randolph Road, SE
Albuquerque, NM 87106

Naval Research Laboratory — 10
ATTN: Dr. Martin Lampe (4790)
Dr. J. Robert Greig (4763)
Dr. Richard Hubbard (4790)
Dr. A. Wahab Ali (4700.1)
Dr. Robert Pechacek (4760)
Dr. Donald Murphy (4760)
Dr. Richard Fernsler (4770)
Dr. Bertrum Hui (4790)
Dr. Glen Joyce (4790)
Ms. Wilma Brizzi (4790)
4555 Overlook Avenue, SW
Washington, DC 20375

Naval Surface Weapons Center — 9
White Oak Laboratory
ATTN: Dr. Eugene E. Nolting (R401)
Ms. Beverly McLean (R401)
Dr. H.C. Chen (R41)
Dr. Han S. Uhm (R41)
Dr. Ralph Fiorito (R41)
Dr. John Smith (R41)
Dr. Donald Rule (R41)
Dr. M.J. Rhee (R41)
10901 New Hampshire Avenue
Silver Springs, MD 20903–5000

Office of Naval Research — 1
ATTN: CDR R. Swafford
800 N. Quincy Street
Arlington, VA 22217

LT COL E.W. Pogue — 1
Strategic Defense Initiative Office
The Pentagon
Office of Secretary of Defense
Washington, DC 20301–7100

Sandia National Laboratory 1
ATTN: Dr. Michael Mazarakis (1272)
P.O. Box 5800
Albuquerque, NM 87185

Sandia National Laboratories 1
ATTN: Dr. Carl Ekdahl (1272)
P.O. Box 5800
Albuquerque, NM 87185

Science Applications International Corp. 1
ATTN: Dr. R. Leon Feinstein
5150 El Camino Real, Suite B–31
Los Altos, CA 94022

SRI International 1
ATTN: Dr. Donald J. Eckstrom
333 Ravenswood Avenue
Menlo Park, CA 94025

CAPT Kurt Stevens 1
AFTAC/TX OP
Patrick AFB
Patrick, FL 32925

Strategic Defense Initiative Organization 1
Directed Energy Weapons Office
The Pentagon
ATTN: LTCOL Richard L. Gullickson
Office of the Secretary of Defense
Washington, D.C. 20301–7100

Admiral R.L. Topping 1
Space and Naval Warfare Systems Command
SPAWAR–06
Washington, D.C. 20363–5100

LCDR E. Turner
Naval Sea Systems Command
(PMW–145)
SPAWAR
Washington, D.C. 20363–5000 1

Research Administration
Code 012
Naval Postgraduate School
Monterey, CA 93943 1